CEAS EuroGNC 2019
"Conference on Guidance, Navigation and Control"
3-5 April 2019 @ Politecnico di Milano, Milan, Italy.

CEAS-GNC-2019-046

Nonlinear Disturbance Observer-Based Attitude Controller for Exoatmospheric DACS Type Missile Considering Seeker's Field-of-View Limit

Jaeho Lee, Seokwon Lee, and Youdan Kim

Abstract A nonlinear disturbance observer-based attitude controller is proposed for an exoatmospheric divert and attitude control system (DACS) type missile with a seeker's narrow field-of-view to maintain a lock-on condition. Dynamic model of the DACS type missile is derived considering varying center of mass caused by fuel consumption of the thrusters. Based on the separation between the translational and rotational motions of the missile in the exoatmospheric environment, attitude controller is designed based on the nominal missile dynamic model using the sliding mode control scheme. To compensate the effects of varying center of mass, the nonlinear disturbance observer for high-order disturbances is designed. Numerical simulation is performed considering the narrow field-of-view and varying center of mass to demonstrate the performance of the proposed controller.

1 Introduction

Anti-ballistic missile defense system aims to intercept the ballistic target at exoatmospheric altitude to eliminate the threats from the target. The operation of the missile in exoatmospheric environment provides several technical challenges [1]. First, the aerodynamic control using the missile's fin is not applicable, and therefore thrust-based control such as the divert and attitude control system (DACS) should be utilized. Second, the closing speed between the missile and the target is very high, and therefore the missile should achieve "hit-to-kill" interception. This means that the missile physically collides with the target using its kinetic energy, which increases the likelihood of the defense. Third, if the missile is equipped with a strapdown seeker, then the missile may have a narrow field-of-view limit to secure a sufficient detectable range of the seeker for high closing velocity. Therefore,

Jaeho Lee, Seokwon Lee, and Youdan Kim
Department of Mechanical and Aerospace Engineering, Seoul National University, Seoul 08826, Republic of Korea, e-mail: akfksem@snu.ac.kr; blueswl@snu.ac.kr; ydkim@snu.ac.kr

to maintain the target within the field-of-view of the seeker, precise control of the missile attitude is essential.

Several research on the guidance law taking into account the field-of-view limit of the seeker have been carried out based on the switching approach [2–4]. These studies considered the missile as a point mass, and therefore the missile body axis coincides with the velocity axis under the assumption that the missile performs maneuver at low angle-of-attack in atmospheric environment. On the other hand, the translational and rotational motions of the missile can be separated in exoatmospheric environment. Therefore, in the exoatmospheric environment, guidance laws which is specific to the target interception can be utilized regardless of the field-of-view limit of the seeker by controlling the attitude of the missile properly. Recently, several attitude controllers considering the separation between the translational and rotational motions in the exoatmospheric environment were proposed [5–7]. Especially, a sliding mode-based attitude controller for the DACS type missile was designed, which has a two-loop structure [7]. However, these studies did not consider a variation of the center of mass of the missile caused by the fuel consumption of the DACS thrusters although it may cause a severe performance degradation of the attitude controller.

In this study, a nonlinear disturbance observer-based attitude controller is designed considering the varying center of mass of the missile caused by fuel consumption of the DACS. The translational and rotational motions of the DACS type missile are modeled considering the varying center of mass, where the DACS consists of two thruster systems, i.e., the divert control system (DCS) and attitude control system (ACS). Using the sliding mode control scheme, attitude controller is desinged as a two-loop structure, i.e., the outer- and inner-loops, which deal with the Euler angles and angular velocities, respectively. The outer-loop generates the angular velocity commands to maintain the lock-on condition using the seeker's information, and the inner-loop generates the commands of the ACS thrust forces corresponding to the angular velocity commands from the outer-loop. To deal with the various types of variations of the center of mass and guidance acceleration commands, nonlinear disturbance observer guaranteeing the estimation performance for high-order disturbances is designed. By combining the designed controller and observer, the disturbance observer-based attitude controller for an exatmospheric DACS type missile is proposed. Numerical simulation for the exoatmospheric engagement against the ballistic target is performed to demonstrate the performances of the designed attitude controller and disturbance observer, where the narrow field-of-view of the seeker and varying center of mass are considered.

The remainder of the paper is organized as follows. Section 2 presents problem formulation including the definition of the look angle of the seeker and the dynamic model of the exatmospheric DACS type missile. In Sect. 3, disturbance observer-based attitude controller is designed, and the results of the numerical simulation are provided in Sect. 4. Finally, concluding remarks are given in Sect. 5.

2 Problem Formulation

2.1 Look Angle of the Seeker

Because the translational and rotational motions of the missile can be separated in exoatmospheric environment, the missile body axis cannot be assumed to be aligned with the velocity axis. Therefore, in this study, the look angle of the seeker is defined as the magnitude of angle between the x-axes of the missile body and line-of-sight (LOS) coordinate systems. Figure 1 shows the definition of the look angle of the seeker, where the superscripted $[I]$, $[B]$, $[L]$, and $[V_M]$ denote the inertial, missile body, LOS, and missile velocity coordinate systems, respectively, and σ is the look angle of the seeker. Based on the definition of the look angle, the lock-on condition against the target can be maintained by regulating the look angle rapidly.

2.2 Missile Dynamic Model

In this study, translational and rotational motions of the DACS type missile are modeled for the configuration of the DACS thrusters with varying center of mass of the missile. Figure 2 shows the configuration of the DACS type missile considered in this study, where $T_{D_{Y,k}}$ and $T_{D_{Z,k}}$, $k = 1, 2$, are the DCS thrust forces, T_{A_k}, $k = 1, \cdots, 6$, is the ACS thrust force, l_d is the distance between the centers of the DCS and ACS, l_a is the distance between the ACS thrusters, and $x_{CM} = [\varepsilon_x \ \varepsilon_y \ \varepsilon_z]^T$ is the position vector of the center of mass. Using the DCS and ACS thrust forces, the virtual thrust forces can be defined as follows,

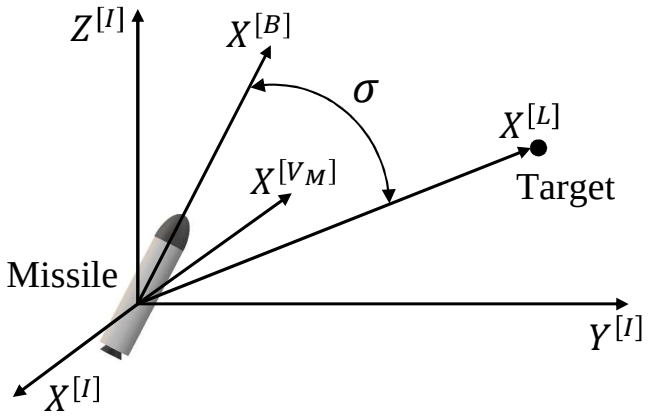

Fig. 1 Definition of the look angle of the seeker

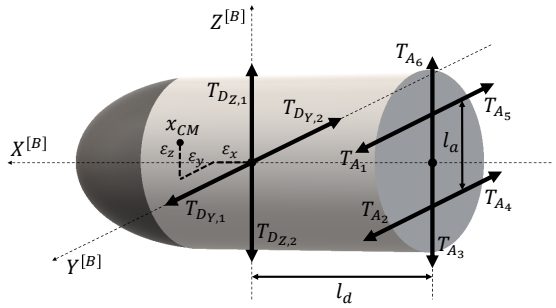

Fig. 2 Configuration of the DACS type missile

$$T_{D_Y} = T_{D_{Y,1}} - T_{D_{Y,2}} \tag{1}$$

$$T_{D_Z} = T_{D_{Z,1}} - T_{D_{Z,2}} \tag{2}$$

$$T_{A_L} = -T_{A_1} + T_{A_2} - T_{A_4} + T_{A_5} \tag{3}$$

$$T_{A_M} = -T_{A_3} + T_{A_6} \tag{4}$$

$$T_{A_N} = -T_{A_1} - T_{A_2} + T_{A_4} + T_{A_5} \tag{5}$$

where T_{D_Y} and T_{D_Z} represent the thrust forces of the DCS generating the z- and y-axis forces, respectively, and T_{A_L}, T_{A_M}, and T_{A_N} represent the thrust forces of the ACS generating the roll, pitch, and yaw moments, respectively. Using Eqs. (1)-(5), translational motion of the missile can be expressed as

$$a_z = \frac{T_{D_Z} + T_{A_M}}{m} \tag{6}$$

$$a_y = \frac{T_{D_Y} - T_{A_N}}{m} \tag{7}$$

where a_z and a_y are the pitch and yaw accelerations, respectively, and m is the mass of the missile. To derive the rotational dynamic model of the missile, following assumptions are considered.

Assumption 1: The products of inertia of the missile body caused by a violation of axial symmetry around x-axis are neglected.

Assumption 2: DCS generates proper thrust forces corresponding to the guidance acceleration commands.

Under *Assumption 1*, the moment of inertia matrix of the missile body can be expressed as

$$\mathbf{I} = \begin{bmatrix} I_{xx} & 0 & 0 \\ 0 & I_{yy} & 0 \\ 0 & 0 & I_{zz} \end{bmatrix} \tag{8}$$

where I_{xx}, I_{yy}, and I_{zz} are principal moments of inertia of the missile. The rotational motion of the missile is governed by the following differential equation.

$$\dot{\omega} = \mathbf{I}^{-1}\left(\mathbf{M} - \omega \times \mathbf{I}\omega\right) \tag{9}$$

where $\omega = [p\ q\ r]^T$ is the angular velocity vector, and $\mathbf{M} = [L\ M\ N]^T$ is the external moment vector. Considering the configuration of the DACS type missile in Fig. 2, the components of the external moment vector can be obtained as follows,

$$L = \frac{1}{2} l_a T_{A_L} - \varepsilon_y T_{A_M} - \varepsilon_z T_{A_N} - \varepsilon_y T_{D_Z} + \varepsilon_z T_{D_Y} \tag{10}$$

$$M = (l_d + \varepsilon_x) T_{A_M} + \varepsilon_x T_{D_Z} \tag{11}$$

$$N = (l_d + \varepsilon_x) T_{A_N} - \varepsilon_x T_{D_Y} \tag{12}$$

Under *Assumption 2*, the DCS thrust forces can directly be calculated using Eqs. (6) and (7) as follows,

$$T_{D_Z} = m a_{z,c} - T_{A_M} \tag{13}$$

$$T_{D_Y} = m a_{y,c} + T_{A_N} \tag{14}$$

where $a_{z,c}$ and $a_{y,c}$ are the pitch and yaw guidance acceleration commands with respect to the missile body coordinate system. Substituting Eqs. (13) and (14) into Eqs. (10)-(12), the external moments of the missile body can be rewritten as

$$L = \frac{1}{2} l_a T_{A_L} - m a_{z,c} \varepsilon_y + m a_{y,c} \varepsilon_z \tag{15}$$

$$M = l_d T_{A_M} + m a_{z,c} \varepsilon_x \tag{16}$$

$$N = l_d T_{A_N} - m a_{y,c} \varepsilon_x \tag{17}$$

Substituting Eqs. (8) and (15)-(17) into Eq. (9), rotational dynamic model of the missile can be obtained as follows,

$$\dot{p} = \frac{1}{I_{xx}} \left(\frac{1}{2} l_a T_{A_L} - m a_{z,c} \varepsilon_y + m a_{y,c} \varepsilon_z \right) \tag{18}$$

$$\dot{q} = \frac{1}{I_{yy}} \left\{ (I_{zz} - I_{xx})\, pr + l_d T_{A_M} + m a_{z,c} \varepsilon_x \right\} \tag{19}$$

$$\dot{r} = \frac{1}{I_{zz}} \left\{ (I_{xx} - I_{yy})\, pq + l_d T_{A_N} - m a_{y,c} \varepsilon_x \right\} \tag{20}$$

To represent the attitude of the missile body, Euler angles from the reference coordinate system to the missile body coordinate system are introduced with the sequence of z-, -y-, and x-axes. The relationship between the Euler angles and the angular velocities can be represented as follows,

$$\dot{\phi} = p - q\sin\phi\tan\theta - r\cos\phi\tan\theta \tag{21}$$

$$\dot{\theta} = q\cos\phi - r\sin\phi \tag{22}$$

$$\dot{\psi} = q\sin\phi\sec\theta + r\cos\phi\sec\theta \tag{23}$$

where ϕ, θ, and ψ are the roll, pitch, and yaw Euler angles of the missile body, respectively. Note from the sequence of the Euler angle that ψ and θ represent the azimuth and elevation angles, respectively, from the inertial coordinate system to the missile body coordinate system.

3 Disturbance Observer-Based Controller Design

In this section, nonlinear disturbance observer-based attitude controller is designed for the exatmospheric DACS type missile. Controlling the attitude of the missile body to maintain the lock-on condition until intercepting the target is the main objective of the controller design. The narrow field-of-view of the seeker and varying center of mass of the missile caused by fuel consumption of the DACS are considered. In this study, the controller structure composed of the sliding mode-based attitude controller and nonlinear disturbance observer is proposed as shown in Fig. 3, where p_c, q_c, and r_c are the roll, pitch, and yaw angular velocity commands, respectively, and $\hat{d}_1$, $\hat{d}_2$, and $\hat{d}_3$ are the estimates of the disturbances. Attitude controller is designed for the missile dynamic model without considering the variation of the center of mass, i.e., $x_{CM} = [0\ 0\ 0]^T$. Also, Euler angles and angular velocities are separately controlled by the outer- and inner-loop controllers, respectively, to efficiently handle the states of different frequencies and obtain the additional design parameters. Nonlinear disturbance observer is design for high-order disturbances to deal with various types of the guidance acceleration commands. Finally, nonlinear disturbance observer-based attitude controller is designed by combining the sliding mode-based attitude controller with the nonlinear disturbance observer.

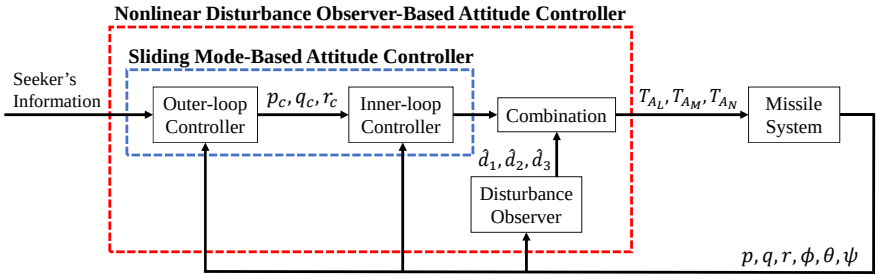

Fig. 3 Block diagram of nonlinear disturbance observer-based attitude controller

3.1 Sliding Mode-Based Attitude Controller Design

3.1.1 Outer-Loop Controller

The outer-loop controller is designed to generate the angular velocity commands maintaining the lock-on condition against the target. Let us define the error vector including the seeker's information as

$$e_o = \begin{bmatrix} e_\phi \\ e_\theta \\ e_\psi \end{bmatrix} = \begin{bmatrix} \phi \\ \theta \\ \psi \end{bmatrix} - \begin{bmatrix} \phi_c \\ \theta_L \\ \psi_L \end{bmatrix} \tag{24}$$

where ϕ_c is the roll angle command, and ψ_L and θ_L are the azimuth and elevation angles, respectively, from the inertial coordinate system to the LOS coordinate system, which can be obtained from the seeker. Note that the look angle of the seeker converges to zero as e_θ and e_ψ converge to zero considering the definition of the look angle of the seeker. To regulate the error vector using the sliding mode control scheme, sliding surfaces of the outer-loop controller are defined as follows,

$$s_\phi = e_\phi + \lambda_\phi \int_0^t e_\phi d\tau \tag{25}$$

$$s_\theta = e_\theta + \lambda_\theta \int_0^t e_\theta d\tau \tag{26}$$

$$s_\psi = e_\psi + \lambda_\psi \int_0^t e_\psi d\tau \tag{27}$$

where λ_ϕ, λ_θ, and λ_ψ are the design parameters which are set to be positive real values. Differentiating Eqs. (25)-(27) with respect to time and substituting Eqs. (21)-(23) into the resulting equations, dynamics of the sliding surface vector of the outer-loop controller can be obtained as follows,

$$\dot{s}_o = F_o - X_o + G_o u_o \tag{28}$$

where $s_o = [s_\phi \; s_\theta \; s_\psi]^T$, $u_o = [p \; q \; r]^T$, and

$$F_o = \begin{bmatrix} \lambda_\phi \phi \\ \lambda_\theta \theta \\ \lambda_\psi \psi \end{bmatrix}, \; X_o = \begin{bmatrix} \dot{\phi}_c + \lambda_\phi \phi_c \\ \dot{\theta}_L + \lambda_\theta \theta_L \\ \dot{\psi}_L + \lambda_\psi \psi_L \end{bmatrix}, \; G_o = \begin{bmatrix} 1 & -\sin\phi\tan\theta & -\cos\phi\tan\theta \\ 0 & \cos\phi & -\sin\phi \\ 0 & \sin\phi\sec\theta & \cos\phi\sec\theta \end{bmatrix}$$

Based on Eq. (28), a sliding mode-based control input of the outer-loop controller is proposed as

$$u_{o,c} = -G_o^{-1}\left(F_o - X_o + K_{o,1} s_o + K_{o,2}\mathrm{sgn}(s_o)\right) \tag{29}$$

where $\mathrm{sgn}(\cdot)$ denotes the sign function, and $K_{o,1}$ and $K_{o,2}$ are the control gain matrices which have positive real diagonal components. To analyze the stability of the

closed-loop system, let us substitute Eq. (29) into Eq. (28).

$$\dot{s}_o = -K_{o,1}s_o - K_{o,2}\text{sgn}(s_o) \tag{30}$$

Now, consider the following Lyapunov candidate function.

$$V_o = \frac{1}{2}s_o^T s_o \tag{31}$$

Taking the time derivative of Eq. (31), we have

$$\dot{V}_o = -s_o^T K_{o,1}s_o - s_o^T K_{o,2}\text{sgn}(s_o) \tag{32}$$

Note from Eq. (32) that the time derivative of the Lyapunov candidate function is negative definite. Therefore, the sliding surfaces of the outer-loop controller converge to zero in finite time, and are maintained thereafter. If the sliding surfaces of the outer-loop controller are maintained to be zero, then the following equalities are also maintained based on Eqs. (25)-(27).

$$\dot{e}_\phi = -\lambda_\phi e_\phi \tag{33}$$

$$\dot{e}_\theta = -\lambda_\theta e_\theta \tag{34}$$

$$\dot{e}_\psi = -\lambda_\psi e_\psi \tag{35}$$

Equations (33)-(35) imply that the look angle of the seeker and the roll angle converge to zero and the roll angle command, respectively.

3.1.2 Inner-Loop Controller

The inner-loop controller is designed to generate the ACS thrust forces for the angular velocity commands generated by the outer-loop controller. Let us define the error vector including the angular velocity commands as

$$e_i = \begin{bmatrix} e_p \\ e_q \\ e_r \end{bmatrix} = \begin{bmatrix} p \\ q \\ r \end{bmatrix} - \begin{bmatrix} p_c \\ q_c \\ r_c \end{bmatrix} \tag{36}$$

Sliding surfaces of the inner-loop controller are also defined as

$$s_p = e_p + \lambda_p \int_0^t e_p d\tau \tag{37}$$

$$s_q = e_q + \lambda_q \int_0^t e_q d\tau \tag{38}$$

$$s_r = e_r + \lambda_r \int_0^t e_r d\tau \tag{39}$$

where λ_p, λ_q, and λ_r are the design parameters which are set to be positive real values. Taking the time derivative of Eqs. (37)-(39) and substituting Eqs. (18)-(20) with $x_{CM} = [0\ 0\ 0]^T$ into the resulting equations, dynamics of the sliding surface vector of the inner-loop controller can be obtained as

$$\dot{s}_i = F_i - X_i + G_i u_i \tag{40}$$

where $s_i = [s_p\ s_q\ s_r]^T$, $u_i = [T_{A_L}\ T_{A_M}\ T_{A_N}]^T$, and

$$F_i = \begin{bmatrix} \lambda_p p \\ \lambda_q q + \frac{I_{zz}-I_{xx}}{I_{yy}} pr \\ \lambda_r r + \frac{I_{xx}-I_{yy}}{I_{zz}} pq \end{bmatrix},\ X_i = \begin{bmatrix} \dot{p}_c + \lambda_p p_c \\ \dot{q}_c + \lambda_q q_c \\ \dot{r}_c + \lambda_r r_c \end{bmatrix},\ G_i = \begin{bmatrix} \frac{1}{2I_{xx}} l_a & 0 & 0 \\ 0 & \frac{l_d}{I_{yy}} & 0 \\ 0 & 0 & \frac{l_d}{I_{zz}} \end{bmatrix}$$

Considering the dynamics of the sliding surface vector of the inner-loop controller, a sliding mode-based control input of the inner-loop is proposed as

$$u_{i,c} = -G_i^{-1} \left(F_i - X_i + K_{i,1} s_i + K_{i,2} \mathrm{sgn}(s_i) \right) \tag{41}$$

where $K_{i,1}$ and $K_{i,2}$ are the control gain matrices which have positive real diagonal components. Substituting Eq. (41) into Eq. (40) yields

$$\dot{s}_i = -K_{i,1} s_i - K_{i,2} \mathrm{sgn}(s_i) \tag{42}$$

Similar to the outer-loop controller design, Eq. (42) guarantees that the errors of the angular velocities converge to zero in finite time.

3.2 Nonlinear Disturbance Observer Design

To compensate the performance degradation due to the change of the center of mass, nonlinear disturbance observer is designed. Especially, in this study, the high-order disturbance observer is considered to deal with several types of uncertainties. The dynamics of the angular velocities with varying center of mass presented in Eqs. (18)-(20) can be rewritten as follows,

$$\dot{\omega} = f(\omega) + G_i u_i + d \tag{43}$$

where

$$f(\omega) = \begin{bmatrix} 0 \\ \frac{I_{zz}-I_{xx}}{I_{yy}} pr \\ \frac{I_{xx}-I_{yy}}{I_{zz}} pq \end{bmatrix},\ d = \begin{bmatrix} d_1 \\ d_2 \\ d_3 \end{bmatrix} = \begin{bmatrix} -\frac{m}{I_{xx}} \left(a_{z,c} \varepsilon_y + a_{y,c} \varepsilon_z \right) \\ \frac{m}{I_{yy}} a_{z,c} \varepsilon_x \\ -\frac{m}{I_{zz}} a_{y,c} \varepsilon_x \end{bmatrix}$$

Now, let us consider a following assumption.

Assumption 3: The disturbance d_k, $k = 1,2,3$, are third-order polynomial function, with respect to time, which are presented as

$$d_k = d_{k,0} + d_{k,1}t + d_{k,2}t^2 + d_{k,3}t^3 \quad \text{for} \quad k = 1,2,3 \tag{44}$$

where $d_{k,0}$, $d_{k,1}$, $d_{k,2}$, and $d_{k,3}$ are unknown constant coefficients.

Under *Assumption 3*, following observer state dynamics and estimation for third-order disturbances are considered [8].

$$\dot{z} = f(\omega) + G_i u_i + \sum_{k=0}^{3} \Gamma_k g_k \tag{45}$$

$$\hat{d} = \sum_{k=0}^{3} \Gamma_k g_k \tag{46}$$

where Γ_0, Γ_1, Γ_2, and Γ_3 are the observer gain matrices which have positive real diagonal components, and

$$g_k = \begin{cases} \omega - z & \text{for} \quad k = 0 \\ \int_0^t g_{k-1} d\tau & \text{for} \quad k = 1,2,3 \end{cases}$$

To analyze the stability of the designed disturbance observer, let us define a disturbance error vector as

$$e_d = \hat{d} - d \tag{47}$$

Taking the time derivative of Eq. (47) and substituting Eqs. (43), (45), and (46) into the resulting equation, we have

$$\begin{aligned} \dot{e}_d &= \dot{\hat{d}} - \dot{d} \\ &= \sum_{k=0}^{3} \Gamma_k \dot{g}_k - \dot{d} \\ &= -\Gamma_0 e_d + \sum_{k=1}^{3} \Gamma_k g_{k-1} - \dot{d} \end{aligned} \tag{48}$$

Taking the time derivatives of Eq. (48) three more times, the fourth derivative of the disturbance error vector with respect to time can be obtained as

$$e_d^{(4)} = -\sum_{k=0}^{3} \Gamma_k e_d^{(3-k)} - d^{(4)} \tag{49}$$

where the superscript (k) denotes the k-th derivative with respect to time. Because $d^{(4)}$ is zero under *Assumption 3*, Eq. (49) can be rewritten as follows,

$$e_d^{(4)} + \Gamma_0 e_d^{(3)} + \Gamma_1 \ddot{e}_d + \Gamma_2 \dot{e}_d + \Gamma_3 e_d = 0 \tag{50}$$

Because Γ_0, Γ_1, Γ_2, and Γ_3 are the diagonal matrices which have positive real components, Eq. (50) implies that the disturbance error vector converges to zero in finite time.

3.3 Nonlinear Disturbance Observer-Based Attitude Controller

Combining the sliding mode-based attitude controller with the high-order disturbance observer, the nonlinear disturbance observer-based attitude controller for the exoatmospheric DACS type missile is designed. Using the inner-loop control input, Eq. (41), and disturbance estimate vector, Eq. (46), the nonlinear disturbance observer-based control input can be obtained as follows,

$$u_c = u_{i,c} - G_i^{-1}\hat{d} \tag{51}$$

Substituting Eq. (51) into Eq. (43), the closed-loop dynamics of the angular velocity vector can be obtained as

$$\dot{\omega} = f(\omega) + G_i u_{i,c} + e_d \tag{52}$$

Because the disturbance error vector converges to zero in finite time and the sliding mode-based inner-loop controller guarantees the convergence of the angular velocity errors on Eq. (52) with $e_d = [0\ 0\ 0]^T$, the designed nonlinear disturbance observer-based attitude controller can be operated satisfactorily for the exoatmospheric DACS type missile with varying center of mass.

4 Numerical Simulation

In this section, numerical simulation is performed to demonstrate the performance of the proposed controller for the DACS type missile to intercept the target in exoatmospheric environment. The physical parameters of the missile used in the simulation is summarized in Table. 1. The DACS thrusters are modeled as a first-order system with a 0.01 time constant, and the maximum thrust forces of the DCS and ACS are set to be $\pm$10g and $\pm$3g, respectively. Figure 4 shows the initial engagement geometry of the simulation, where the superscripted $[V_T]$ denotes the target velocity coordinate system, the subscripted 0 denotes the initial value, and ψ_{L,V_T} and θ_{L,V_T}

Table 1 Physical parameters of the missile

Parameter	m [kg]	l_a [m]	l_d [m]	I_{xx} [kg$\cdot$m^2]	I_{yy} [kg$\cdot$m^2]	I_{zz} [kg$\cdot$m^2]
Value	64	0.2	0.6	2.88	11.89	11.89

are the azimuth and elevation angles, respectively, from the LOS coordinate system to the missile velocity coordinate system. Note that x-axes of the missile body and velocity coordinate systems are aligned in the initial stage. The initial conditions of the missile and the target are summarized in Table. 2, where $[X_M\ Y_M\ Z_M]^T$ and $[X_T\ Y_T\ Z_T]^T$ are the position vectors of the missile and target, respectively, with respect to the reference coordinate system, and V_M and V_T are total velocities of the missile and target, respectively. The field-of-view limit of the seeker is set to be ± 4 deg, and the initial look angle is 2.83 deg, and therefore the lock-on condition is satisfied in the initial time. In the simulation, a following 3-dimensional pure pursuit navigation guidance law with respect to the missile velocity coordinate system is used to generate the guidance acceleration commands of the pitch and yaw accelerations [9].

$$a_{z,c}^{[V_M]} = -N_g V_M \dot{\lambda}_y \cos\psi_{L,V_M} \tag{53}$$

$$a_{y,c}^{[V_M]} = -N_g V_M \dot{\lambda}_y \sin\theta_{L,V_M} \sin\psi_{L,V_M} + N_g V_M \dot{\lambda}_z \cos\theta_{L,V_M} \tag{54}$$

where N_g is the navigation constant which are set to be 6, λ_y and λ_z are the y and z components of the LOS vector with respect to the reference coordinate system, respectively, and ψ_{L,V_M} and θ_{L,V_M} are the azimuth and elevation angles, respectively, from the LOS coordinate system to the missile velocity coordinate system. And, all

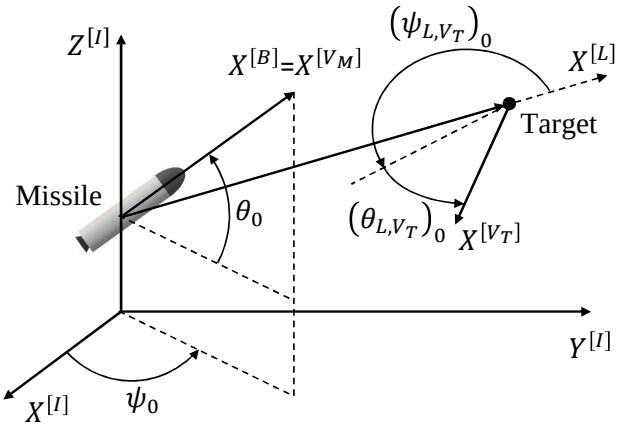

Fig. 4 Initial engagement geometry of the simulation

Table 2 Initial conditions of missile and target

$[X_M\ Y_M\ Z_M]_0^T$ [km]	$[X_T\ Y_T\ Z_T]_0^T$ [km]	$[\phi\ \theta\ \psi]_0^T$ [deg]	$[\psi_{L,V_T}\ \theta_{L,V_T}]_0^T$ [deg]	V_M, V_T [km/s]
$[0\ 0\ 100]^T$	$[0\ 25\sqrt{3}\ 125]^T$	$[2\ 27.98\ 87.74]^T$	$[-178.5\ -2.5]^T$	4.5, 2.5

design parameters of the sliding surfaces are set to be 1, and the control and observer gain matrices are set as

$$K_{o,1} = \begin{bmatrix} 6 & 0 & 0 \\ 0 & 1 & 0 \\ 0 & 0 & 1 \end{bmatrix}, \quad K_{o,2} = \begin{bmatrix} 6 & 0 & 0 \\ 0 & 1 & 0 \\ 0 & 0 & 1 \end{bmatrix}, \quad K_{i,1} = \begin{bmatrix} 15 & 0 & 0 \\ 0 & 10 & 0 \\ 0 & 0 & 10 \end{bmatrix}, \quad K_{i,2} = \begin{bmatrix} 15 & 0 & 0 \\ 0 & 10 & 0 \\ 0 & 0 & 10 \end{bmatrix}$$

$$\Gamma_0 = \begin{bmatrix} 18 & 0 & 0 \\ 0 & 20 & 0 \\ 0 & 0 & 20 \end{bmatrix}, \quad \Gamma_1 = \begin{bmatrix} 8 & 0 & 0 \\ 0 & 8 & 0 \\ 0 & 0 & 8 \end{bmatrix}, \quad \Gamma_2 = \begin{bmatrix} 2 & 0 & 0 \\ 0 & 2 & 0 \\ 0 & 0 & 2 \end{bmatrix}, \quad \Gamma_3 = \begin{bmatrix} 0.5 & 0 & 0 \\ 0 & 0.5 & 0 \\ 0 & 0 & 0.5 \end{bmatrix}$$

In the simulation, the sign function is replaced with the arctangent function to avoid the chattering phenomenon [10]. Figures 5-10 show the results of the simulation for the case of the sliding mode-based controller with and without the nonlinear disturbance observer. Figure 5 presents the trajectories of the missile and target, where the solid line represents the trajectory of the missile and the dashed line represents the trajectory of the target. The miss distance and altitude are 0.53m and 115.41km, respectively, when the simulation ends at 7.13 seconds. Figure 6 shows the time histories of components of the center of mass position vector, which are generated using the time histories of the DCS thrust forces. Because the translational motion of the missile is separated from the rotational motion in the exoatmospheric environment, the sliding mode controllers with and without the disturbance observer show the same results of the trajectory and DCS thrust forces. Figure 7 presents the time histories of the look angle and ACS thrust forces, where the solid and dash-dotted lines represent the responses of the sliding mode-based controller with and without the disturbance observer, respectively. While the lock-on condition of the controller with the disturbance observer is satisfied until intercepting the target, the

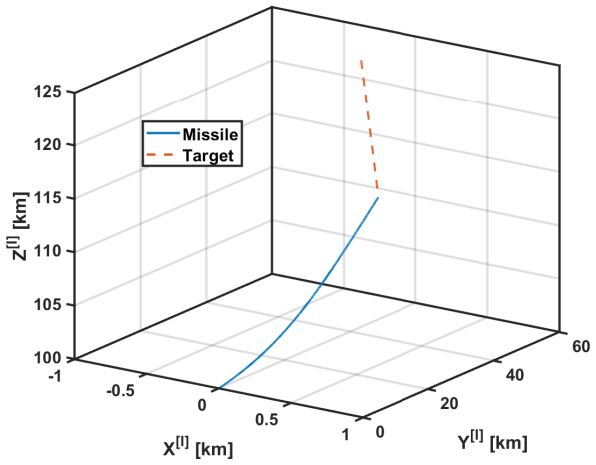

Fig. 5 Trajectories of the missile and target

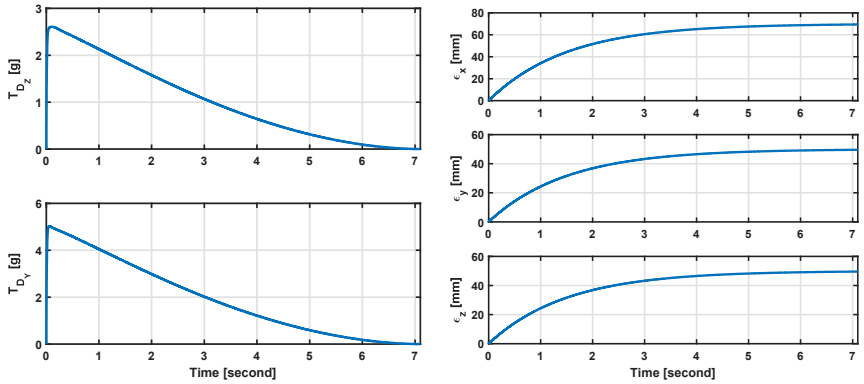

Fig. 6 Time histories of the DCS thrust forces (left) and center of mass components (right)

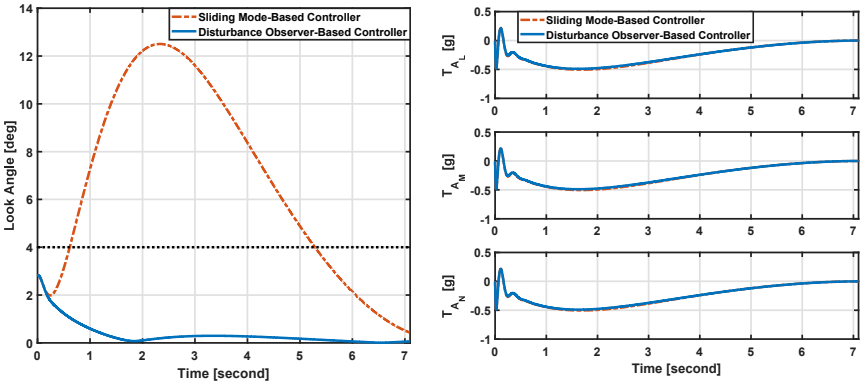

Fig. 7 Time histories of the look angle (left) and ACS thrust forces (right)

look angle of the sliding mode-based controller without the disturbance observer quickly escapes from the seeker's field-of-view. The ACS thrust forces of the two controllers are almost identical, because the magnitude of the inner-loop control input is dominant in the disturbance observer-based controller presented in Eq. (51).

Figures 8 and 9 show the time histories of the Euler angles and angular velocities, respectively, for the two controllers, where the solid line represents the responses of the states and the dashed line represents the responses of the commands. As shown in the responses of the Euler angle and angular velocities, the sliding mode based-controller without the disturbance observer cannot show the sufficient tracking performance. On the other hand, the disturbance observer based-controller shows the satisfactory tracking performances for both Euler angles and angular velocities. Figure 10 presents the time histories of the true and estimated disturbances,

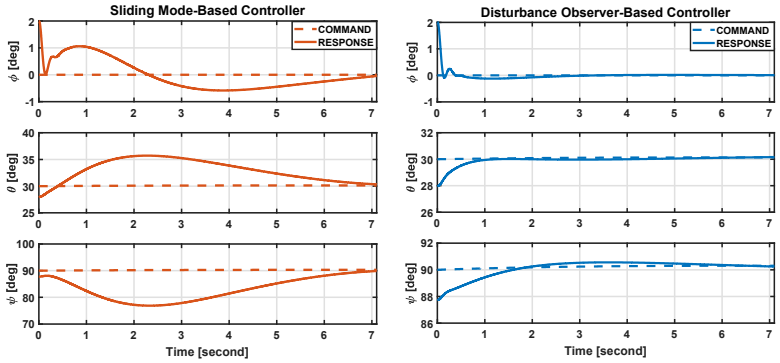

Fig. 8 Time histories of the Euler angles

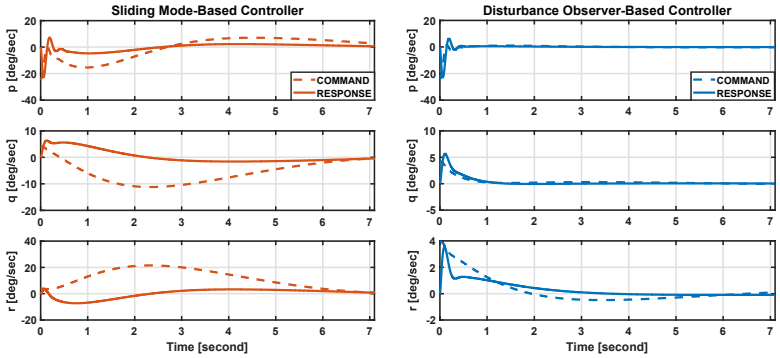

Fig. 9 Time histories of the angular velocities

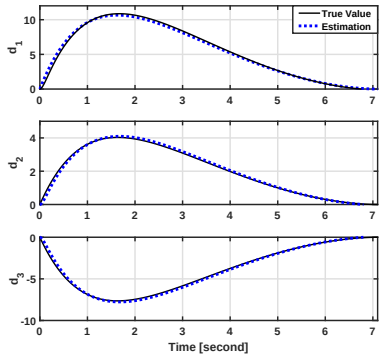

Fig. 10 Time histories of the disturbance components

which shows that the nonlinear disturbance observer has a satisfactory estimating performance for high-order disturbances. In summary, for the exoatmospheric engagement, the disturbance observer-based attitude controller maintains the lock-on condition until intercepting the target by controlling the attitude of the missile properly, while the sliding mode-based controller without the disturbance observer does not intercept the target.

5 Conclusion

Disturbance observer-based attitude controller for an exoatmospheric divert and attitude control system (DACS) type missile was proposed considering a narrow field-of-view of the seeker. The dynamic model of the DACS type missile was derived considering the varying center of mass caused by fuel consumption. The sliding mode-based attitude controller was designed based on the missile dynamic model without the variation of the center of mass. Then, the nonlinear high-order disturbance observer was designed to deal with the several types of variations of the center of mass. The disturbance observer-based attitude controller was synthesized by combining the designed sliding mode-based controller and disturbance observer. Numerical simulation was performed for the exoatmospheric engagement to demonstrate the performance of the proposed controller. The simulation results showed that the small variation of the center of mass due to fuel consumption has a large effect on the intercepting the ballistic target, especially for the missile equipped with a strapdown seeker having narrow field-of-view. The simulation results also emphasized that the variation of the center of mass should be compensated by the disturbance observer.

Acknowledgements This work was conducted as High-Speed Vehicle Research Center of KAIST with the support of Defense Acquisition Program Administration and Agency for Defense Development under Contract UD170018CD.

References

[1] Yingbo H, Yong Q (2003) THAAD-Like High Altitude Theater Missile Defense: Strategic Defense Capability and Certain Countermeasures Analysis. Science and Global Security 11(2-3):151-202

[2] Sang DK, Tahk MJ (2009) Guidance Law Switching Logic Considering the Seeker's Field-of-View Limits. Proceedings of the Institution of Mechanical Engineers - Part G: Journal of Aerospace Engineering 223(8):1049-1058

[3] Lee CH, Hyun C, Lee JG, Choi JY, Sung SK (2013) A Hybrid Guidance Law for a Strapdown Seeker to Maintain Lock-on Conditions against High Speed Targets. Journal of Electrical Engineering and Technology 8(1):190-196

[4] Jeon IS, Lee JI (2017) Impact-Time-Control Guidance Law with Constraints on Seeker Look Angle. IEEE Transactions on Aerospace and Electronic Systems 53(5):2621-2627
[5] Andrieu V, Lahanier HP (2006) Exoatmospheric Interception Problem Solved Using Output Feedback Law. Systems and Control Letters 55(8):633-639
[6] Joner S, Quinquis I (2006) Control of an Exoatmospheric Kill Vehicle with a Solid Propulsion Attitude Control System. AIAA Guidance, Navigation, and Control Conference, Keystone, CO
[7] Lee J, Kim Y (2017) Exoatmospheric DACS Type Missile Controller Based on Sliding Mode Control Considering the Seeker's Field-of-View Limit. Euro GNC 2017 - 4th CEAS Specialist on Guidance, Navigation, and Control, Warsaw, Poland
[8] Kim KS, Rew KH, Kim S (2011) Disturbance Observer for Estimating Higher Order Disturbances in Time Series Expansion. IEEE Transactions on Automatic Control 55(8):1905-1911
[9] Song SH, Ha IJ (1994) A Lyapunov-Like Approach to Performance Analysis of 3-Dimentional Pure PNG Laws. IEEE Transactions on Aerospace and Electronic Systems 30(1):238-248
[10] Thukral A, Innocenti M (1998) A Sliding Mode Missile Pitch Autopilot Synthesis for High Angle of Attack Maneuvering. IEEE Transactions on Control System Technology 6(3):359-371